

## Acid Hydrolysis of Sargassum Fluitans and Sargassum Natans using Iron and Nickel Phosphate-based Nanocatalysts

Salma Luz Torres Mar, José Aarón Melo Banda, David Macías Ferrer, Rebeca Silva Rodrigo, Nancy Patricia Díaz Zavala, Oscar Morelos Santos, Mayda Lam Maldonado

*División de Estudios de Posgrado e Investigación, Instituto Tecnológico de Ciudad Madero, Juventino Rosas y Jesús Urueta S/N, Col. Los Mangos, Cd. Madero, Tamaulipas, C.P. 89440, México.*

*Corresponding Author: david.mf@cdmadero.tecnm.mx*

Date of Submission: 12-02-2026

Date of Acceptance: 25-02-2026

**ABSTRACT:** In this work, Fe, Ni, and FeNi phosphate nanoparticles were synthesized by the thermal decomposition of the organometallic salts  $\text{Fe}(\text{acac})_3$  and  $\text{Ni}(\text{acac})_2$ , using oleylamine and oleic acid as solvent and stabilizer, respectively, and triphenylphosphine as a phosphorus precursor. The aim was to apply these nanoparticles in the acid hydrolysis of sargassum fluitans and natans types. The nanomaterials were characterized using XPS, FTIR, DLS, SEM and XRD. The results showed the presence of PO, FeO, and NiO bonds in catalytic nanoparticles in the 40–100 nm range. The FeNi phosphate nanoparticles exhibited the highest conversion rate of carbohydrates (glucose, xylose, fucose, and mannitol) at 43%, making them viable for use in the production of green fuels.

**KEYWORDS:** Sargassum Fluitans, Sargassum Natans, Nanocatalysts, Iron, Nickel, acid hydrolysis.

### I. INTRODUCTION

Acid hydrolysis of sargassum is a process used to break down the organic matter of sargassum (seaweed) into simpler components, primarily sugars, through the action of an acid at high temperatures. This process yields valuable compounds that can be used in various applications, such as the production of biofuels, bioplastics, and other chemicals. The catalytic process in sargassum decomposition involves the use of catalysts to accelerate the degradation of the organic matter, transforming it into simpler or more useful compounds. Catalysts can reduce decomposition time, lower the temperature required for the process, and increase the yield of desired products such as bio-oil or biogas, which are useful to society and industry [1-3]. Several research projects have been conducted on this topic in recent years. Stefanou G. et al., synthesized 4 and 5 nm Fe-Ni nanoparticles

using the organometallic salts  $\text{Fe}(\text{acac})_3$  and  $\text{Ni}(\text{acac})_2$ , which were magnetically mixed with oleylamine as a stabilizer and polyethylene glycol as a solvent [4]. Perera S. et al., synthesized FeP nanoparticles with an average size of  $4.65 \pm 0.74$  nm by thermal decomposition.  $\text{Fe}(\text{acac})_3$  was used as the iron precursor, and phosphorus was added by incorporating triphenylphosphine and dodecylamine [5]. Yoon K. et al., obtained FeNiP nanorods with a uniform size of 4 x 16 nm. Two FeP and NiP complexes were prepared separately. The FeP complex was prepared by mixing  $\text{Fe}(\text{CO})_5$  and trioctylphosphine at 130°C, then the mixture was heated to 315°C [6]. Kawaroe M. et al., for their part, obtained a 30.5% conversion of sargassum carbohydrates using small concentrations of sulfuric acid [7]. Based on this background, a new synthesis methodology is proposed using the organometallic salts  $\text{Fe}(\text{C}_5\text{H}_7\text{O}_2)_3$  and  $\text{Ni}(\text{C}_5\text{H}_7\text{O}_2)_2$  as precursors of iron and nickel, respectively, oleic acid and oleylamine as solvents and stabilizers, respectively, and triphenylphosphine ( $\text{C}_{18}\text{H}_{15}\text{P}$ ) as a phosphorus precursor, in order to obtain phosphoric Ni and Fe nanocatalysts and contribute to the optimization of the catalytic process of sargassum decomposition by acid hydrolysis.

### II. EXPERIMENTAL

Phosphorous metal nanoparticles as catalysts were synthesized at the facilities of the Technological Institute of Ciudad Madero, in the Division of Postgraduate Studies and Research (ITCM, Campus III), based on the two-stage thermal decomposition method, one at 200°C for one hour and another at 270°C for 30 min., using appropriate amounts of the organo-metallic salts iron (III) acetylacetonate ( $\text{Fe}(\text{C}_5\text{H}_7\text{O}_2)_3$ ), nickel (II) acetylacetonate ( $\text{Ni}(\text{C}_5\text{H}_7\text{O}_2)_2$ ) as precursors of Iron and Nickel

respectively, oleic acid ( $C_{18}H_{34}O_2$ ) and oleylamine ( $C_{18}H_{35}NH_2$ ) as solvents and stabilizers respectively and triphenylphosphine ( $C_{18}H_{15}P$ ) as a precursor of phosphorus. The purification of the metallic and bimetallic nanoparticles was carried out using acetone ( $C_3H_6O$ ) and chloroform ( $CHCl_3$ ) as dispersants via centrifugation [8]. The sargassum pretreatment was as follows: The sargassum was collected from the beaches of the Mexican Caribbean, specifically Cancún, Quintana Roo, washed, and dried in order to grind it using an 80-mesh sieve to ensure particles of approximately 180

$\mu m$ . In order to break down the complex polymers of the sargassum algal biomass into simpler molecules, the acid hydrolysis of the sargassum with concentrated sulfuric acid (2% v/v) was carried out in an Anton Paar Mod. 4790 reactor, using appropriate amounts of emulsion catalysts based on Fe phosphate, Ni phosphate, and Fe-Ni phosphate nanoparticles (see Figure 1). Figure 2 shows the general scheme for the synthesis of Ni and NiO nanoparticles. This scheme was similarly used in the synthesis of Fe, FeO, and FeNi NPs.

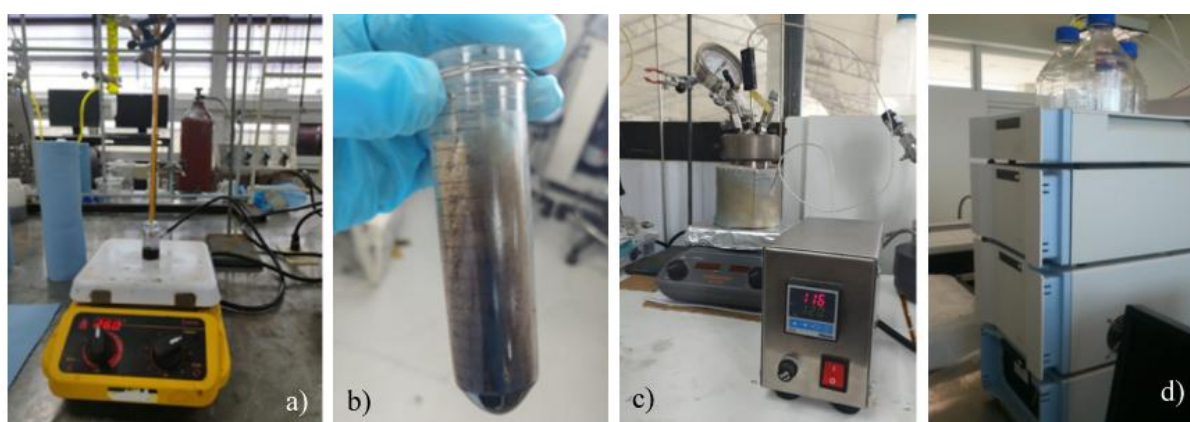


Fig. 1. a) Synthesis of metallic NPs; b) Purification of metallic NPs, c) Acid hydrolysis reaction of Sargassum in a stirred reactor and d) Jasco LC-4000 (HPLC) chromatograph for the determination of carbohydrates and hard fiber of Sargassum.

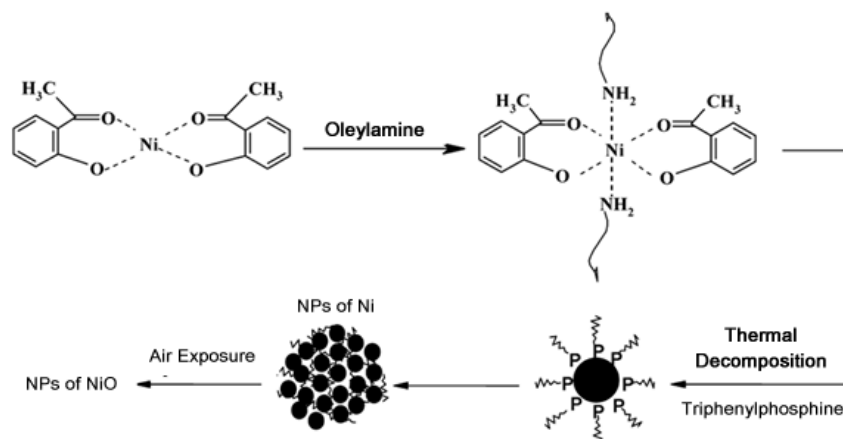


Fig. 2. Synthesis scheme for Ni and NiO nanoparticles.

### III. RESULTS AND DISCUSSIONS

#### FTIR Spectroscopy

The FTIR spectroscopy technique was applied using the Spectrum-100 instrument in the 4000 to 360  $cm^{-1}$  range. Figure 3A shows the absorption bands at 2921  $cm^{-1}$ , 1460  $cm^{-1}$ , and 722

$cm^{-1}$ , corresponding to the vibrations of the C-H,  $CH_3$  (referring to oleic acid) and C-C bonds, respectively [9-11]. Figure 3B presents the absorption bands at 431  $cm^{-1}$  and 405  $cm^{-1}$ , corresponding to the Fe-O bond of the suspended Fe phosphate NPs. Figure 3C presents the absorption band at 465  $cm^{-1}$ , corresponding to the Ni-O bond of the suspended Ni phosphate NPs. Finally, Figure 3D

shows the simultaneous presence of FeO and NiO oxides in the bimetallic FeNi phosphate NPs. These

results are consistent with what has been reported in the literature.

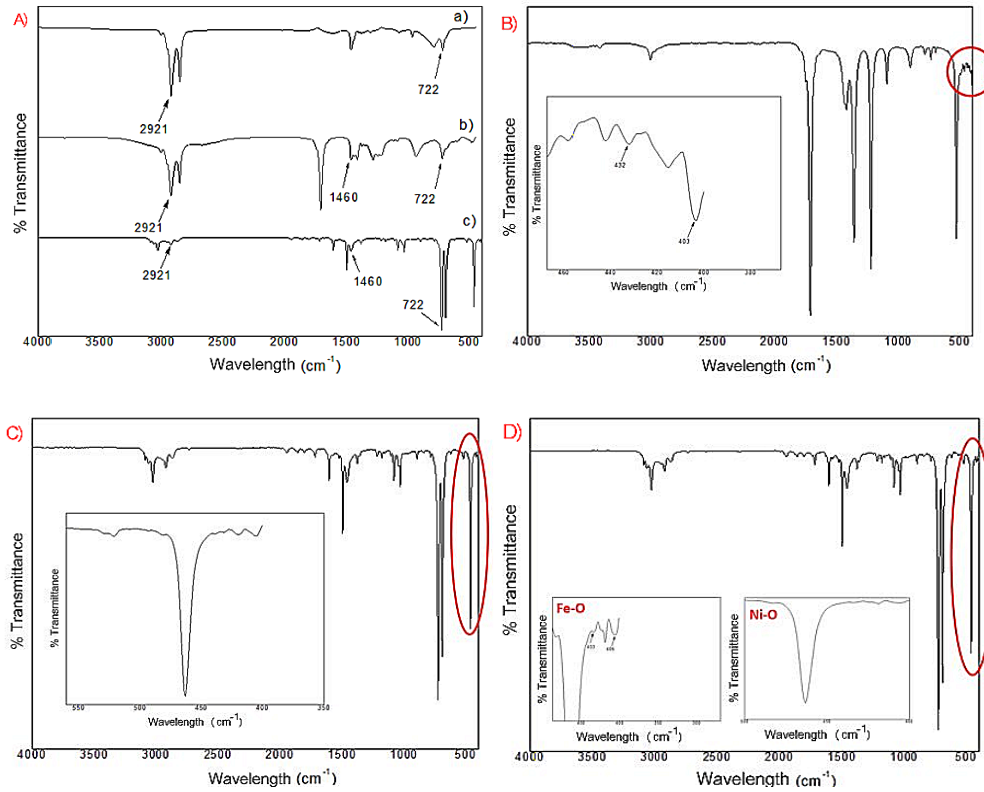


Fig. 3. A) FTIR spectra of a) Oleylamine; b) Oleic acid and c) suspended Ni phosphate NPs; B) suspended Fe phosphate NPs; C) Ni-O bond of the suspended Ni phosphate NPs and D) FeO and NiO oxides in the bimetallic FeNi phosphate NPs

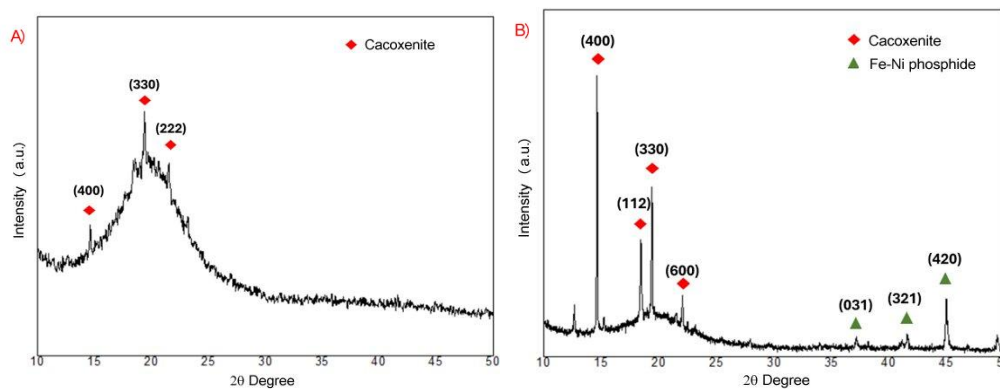


Fig. 4. A) X-ray diffraction pattern of Fe phosphate NPs and B) X-ray diffractogram of iron-nickel metallic nanofibers

### X-ray Diffraction

Figure 4A shows the X-ray diffraction pattern of iron phosphate nanoparticles, revealing a hexagonal structure (space group P63/m, number 176). Reflections at  $2\theta = 14.610^\circ$ ,  $19.384^\circ$ ,  $21.531^\circ$ , and  $23.22^\circ$  are observed, with planes at (400°), (330°), and (222°), respectively, according to the

information reported in chart ICSD 00-014-0331. This diffraction pattern is associated with cacoenite  $\text{Fe}_{24}(\text{PO}_4)_3(\text{OH})_3 \cdot 17\text{H}_2\text{O}$ , a mineral belonging to the iron phosphates with a hexagonal structure. Figure 4B illustrates the X-ray diffractogram of iron-nickel metallic nanofibers. The diffraction pattern shows two crystallographic phases, the first with a hexagonal structure, (space group I-4, number 82),

indicative of cacoxenite, an iron phosphate mineral with reflections  $2\theta = 14.642^\circ, 18.454^\circ, 19.401^\circ$  and  $22.032^\circ$ , assigned to the planes (400), (112), (330) and (600), according to the ICSD card 00-014-0331. The reflections detected at  $2\theta = 35.459^\circ, 41.584^\circ$

and  $45.426^\circ$  in the (-132), (321) and (420) planes, respectively, associated with iron-nickel phosphide with tetragonal structure (space group I-4, number 82), information provided by card ICSD 00-053.[12-13].

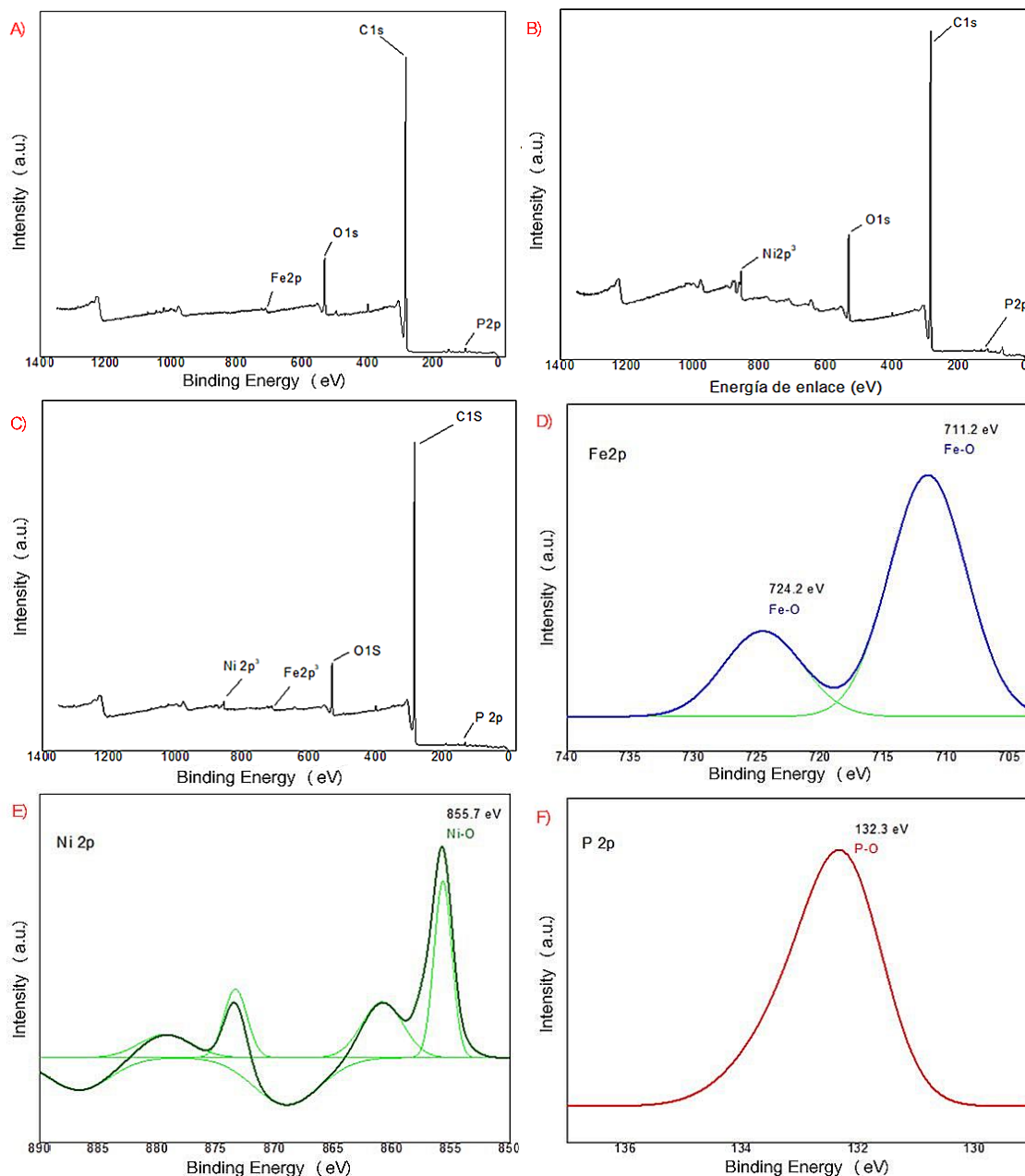


Fig. 5. Survey scan XPS spectra for A) NPs of Fe phosphate; B) NPs of Ni phosphate and C) NPs of FeNi phosphate. Detail XPS spectra of D) Fe 2p; E) Ni 2p and F) P 2p

### XPS Spectroscopy

X-ray photoelectron spectroscopy was applied to iron phosphate, nickel phosphate, and iron-nickel phosphate nanoparticles. This technique

is effective in detecting bonds on the surface of the material being analyzed. Therefore, carbon was detected on the surface of the analyzed

nanomaterials because of the stabilizing agents: oleic acid and oleylamine. These agents prevent nanoparticle growth, which greatly benefits catalytic activity by increasing the contact surface area. Oxygen (O1s) was also detected at 532 eV, belonging to the hydroxyl group (OH). The presence of Fe (see Figure 4A), Ni (see Figure 4B), and both metals (see Figure 4C) was also detected. On the other hand, Figures 4D, 4E and 4F show in detail

the oxidation states of  $\text{Fe}^{2+}$ ,  $\text{Fe}^{3+}$ ,  $\text{Ni}^{2+}$  and  $\text{P}^{5+}$  respectively, which correspond to the bonds of the FeO and NiO oxides and the phosphate radical  $(\text{PO}_4)^{3-}$ . The formation of iron oxides and nickel oxides on the surface of our materials was promoted by the oxygen contained on the surface of the nanocatalyst synthesized in a non-inert environment.[14-16]

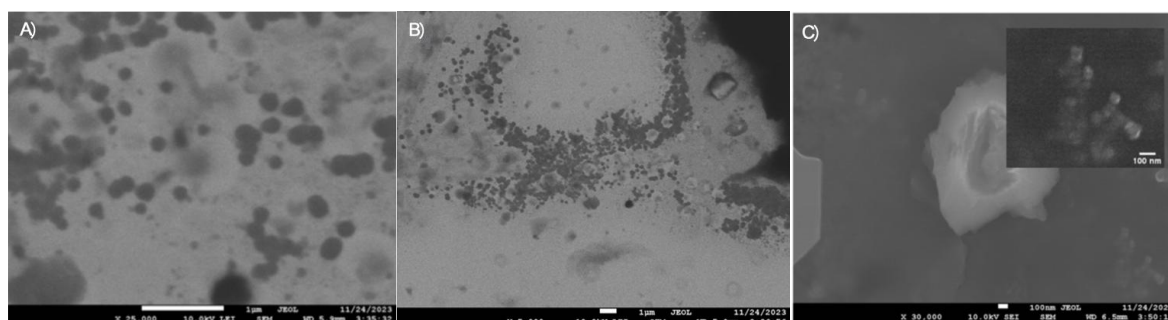


Fig. 5. SEM images of A) NPs of Fe phosphate; B) NPs of Ni phosphate and C) NPs of FeNi phosphate.

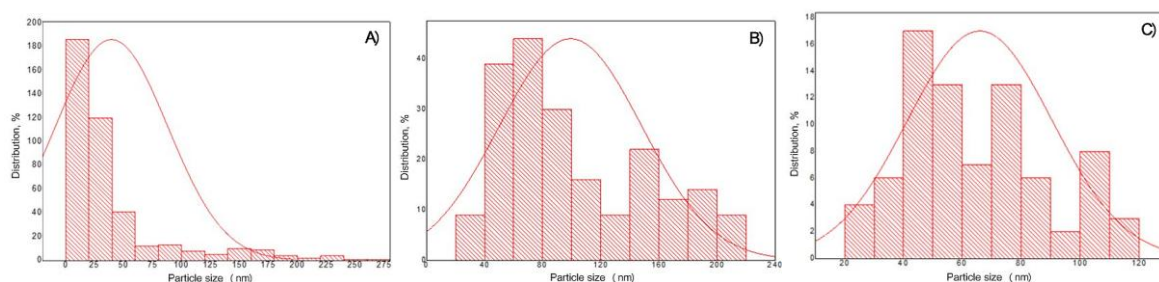


Fig. 6. According to the DLS technique, nanoparticle size distribution histograms were obtained for: a)  $\text{Fe}(\text{PO}_4)_2$ : 40 nm;  $\text{Ni}_3(\text{PO}_4)_2$  NPs: 100 nm; and c)  $\text{Fe}(\text{PO}_4)_2$  and  $\text{Ni}_3(\text{PO}_4)_2$  NPs: 66 nm

### SEM and DLS

To determine the morphology and average size of the nanoparticles, scanning electron microscopy (SEM) and dynamic light scattering (DLS) techniques were applied. According to the microscopic examinations of the samples, spherical, semi-spherical, and some agglomerated nanoparticles were obtained for Fe phosphate, Ni phosphate, and FeNi phosphate (see Figures 5A, 5B, and 5C). Figure 6A shows the histogram of the particle diameter distribution of the iron phosphate nanoparticles, with diameters ranging from 20 to 240 nm, mostly averaging 40 nm. The histogram of the nickel phosphate nanoparticles is shown in Figure 6B. Diameters range from 20 to 220 nm, with an average diameter of 100 nm. Comparing these sizes with the micrograph of nickel phosphate nanoparticles reveals similarities in the sizes of the nanoparticles analyzed by SEM microscopy.

Finally, Figure 6C shows the histogram of the diameter distribution associated with the iron-nickel phosphate nanofibers. Diameters range from 20 to 110 nm, with a majority averaging 40 nm.

### High-Performance Liquid Chromatography

The catalytic acid hydrolysis reaction of sargassum was carried out under controlled temperature conditions ( $120^\circ\text{C}$ ) for 50 min using an Anton Parr model 4790 reactor with a volume of 250 mL. First, a blank reaction was performed in which the reactor was charged with 10 g of ground and sieved sargassum (particle size approximately  $177\ \mu\text{m}$ ), deionized water, and a very small amount of concentrated sulfuric acid (2 mL v/v) to prevent the formation of unwanted reactants such as furfural and 5-hydroxymethylfurfural. The reactor was purged with nitrogen at 8 bar to displace oxygen from the reaction environment and prevent oxidation of the

reactants. Subsequently, three reactions were carried out for 50 min each under the same temperature and pressure conditions using catalysts based on metallic nanoparticles of Fe, Ni, and FeNi phosphates. The

chemical analysis of the reaction products was carried out in a Jesco brand liquid chromatograph Model LC-4000. The results are shown in Table 1.

**Table 1. Products of the acid hydrolysis reaction of sargassum with sulfuric acid and metallic nanoparticles as catalysts.**

Reaction Products	H <sub>2</sub> SO <sub>4</sub>	H <sub>2</sub> SO <sub>4</sub> + NPs Fe(PO) <sub>4</sub>	H <sub>2</sub> SO <sub>4</sub> + NPs Ni <sub>3</sub> ((PO <sub>4</sub> ) <sub>2</sub>	H <sub>2</sub> SO <sub>4</sub> + NPs Fe(PO) <sub>4</sub> + NPs Ni <sub>3</sub> ((PO <sub>4</sub> ) <sub>2</sub>
Glucose	11%	15%	14%	18%
Fucose	4%	5%	7%	8%
Xylose	3%	3%	6%	7%
Mannitol	7%	8%	9%	10%
Total Reducing Sugars	25%	31%	36%	43%
Crude Fiber(Cellulose, lignin etc)	75%	69%	64%	57%

#### IV.CONCLUSIONS

Fe phosphate, Ni phosphate, and Fe-Ni phosphate nanoparticles were successfully synthesized via hydrothermal methods using oleylamine and oleic acid as solvent and stabilizer, respectively, and triphenylphosphine as a phosphorus precursor. These nanoparticles were intended for use as catalysts in the acid hydrolysis of sargassum species *fluitans* and *natans*. Characterization techniques showed that nanoparticles in the 40–100 nm range were obtained, and that the combination of H<sub>2</sub>SO<sub>4</sub> and the bimetallic FeNi nanoparticles resulted in the highest conversion rate of carbohydrates (glucose, fucose, xylose, and mannitol). This may be due to a synergistic effect since, on the one hand, Fe facilitates the transfer of protons towards the most difficult bonds to break in biomass, and on the other hand, Ni is a transition metal with a superior capacity for breaking C-O bonds (glycosidic bonds).

#### ACKNOWLEDGEMENTS

José Aarón Melo Banda gratefully acknowledges the support of Project 23715.25-P of the Proyectos de Investigación Científica e Innovación 2025, funded by Tecnológico Nacional de Mexico as well as, David Macias Ferrer

gratefully acknowledges a scholarship from to Secretaría de Ciencias, Humanidades, Tecnología e Innovación (BP-PA-20240605163515190-8343790) and would like to thanks for technical assistance from the Tecnológico Nacional de México/Instituto Tecnológico de Ciudad Madero/División de Estudios de Posgrado e Investigación/Centro de Investigación en Petroquímica Secundaria, prolongación Ave. Bahía de los Ríos, Parque Industrial de Altamira, Tamaulipas, México.

#### REFERENCES

- [1]. Shi, C., Xu, J., Pan, L., Zhang, X., Zou, J.J. (2021), "Perspective on synthesis of high-energy-density fuels: From petroleum to coal-based pathway", *Chinese Journal of Chemical Engineering*, 35, pp 83–91
- [2]. Alam, M.I., Saha, B. (2015), "Catalysis for the Production of Sustainable Chemicals and Fuels from Biomass", *Sustainable Catalytic Processes*, pp 99-123.
- [3]. Basu, P., (2011), "Biomass gasification and pyrolysis", *Elsevier*, 325-6.
- [4]. Stefanou, G., Sakellari, D., Simeonidis, K., Kalabaliki, T., Angelakeris, M., Dendrinou-Samara, C., Kalogirou, O., (2014), "Tunable AC Magnetic Hyperthermia Efficiency of Ni

- Ferrite Nanoparticles”, *IEEE Transactions on Magnetism*, 50(12), pp 1–7
- [5]. Perera, S. C., Fodor, P. S., Tsoi, G. M., Wenger, L.E., Brock, S.L. (2003). Application of De-silylation Strategies to the Preparation of Transition Metal Pnictide Nanocrystals. The Case of FeP. *Chemistry of Materials*, 15(21), 4034–4038
- [6]. Yoon, K. Y., Jang, Y., Park, J., Hwang, Y., Koo, B., Park, J.-G., Hyeon, T. (2008), “Synthesis of uniform sized bimetallic iron–nickel phosphide nanorods”, *Journal of Solid State Chemistry*, 181(7), 1609–1613
- [7]. Kawaroe M., Prartono T., Kusuma A.H., (2013), “Effect of Acid Concentration on Hydrolysis Efficiency on *Caulerpa racemosa*, *Sargassum crassifolium* and *Gracilaria Salicornia*”, *International Journal of Environment and Bioenergy*, 8(3), 127-134
- [8]. Morelos-Santos, O., De La Torre, A. R., Melo-Banda, J. A., Schacht-Hernández, P., Portales-Martínez, B., Soto-Escalante, I., & José-Yacamán, M. (2022), “A novel direct method in one-step for catalytic heavy crude oil upgrading using iron oxide nanoparticles”, *Catalysis Today*, 392, 60-71.
- [9]. Berthomieu, C., Hienerwadel, R., (2009). “Fourier transform infrared (FTIR) spectroscopy”, *Photosynthesis research*, 101(2), 157-170.
- [10]. Klokkenburg, M., Hilhorst, J., Erné, B. H., (2007), “Surface analysis of magnetite nanoparticles in cyclohexane solutions of oleic acid and oleylamine”, *Vibrational spectroscopy*, 43(1), 243-248.
- [11]. Yang, K., Peng, H., Wen, Y., Li, N., (2010), “Re-examination of characteristic FTIR spectrum of secondary layer in bilayer oleic acid-coated Fe<sub>3</sub>O<sub>4</sub> nanoparticles”, *Applied surface science*, 256(10), 3093-3097.
- [12]. Moore, P.B., Shen, J., (1983), “An X-ray structural study of cacoxenite, a mineral phosphate”, *Nature*, 306(5941), 356-358.
- [13]. Zhou, W., He, W., Zhang, X., Yan, S., Sun, X., Tian, X., & Han, X. (2009). Biosynthesis of iron phosphate nanopowders. *Powder Technology*, 194(1-2), 106-108.
- [14]. Omran, M., Fabritius, T., Elmahdy, A.M., Abdel-Khalek, N.A., El-Aref, M., Elmanawi, A.E.H., (2015), “XPS and FTIR spectroscopic study on microwave treated high phosphorus iron ore”, *Applied surface science*, 345, 127-140.
- [15]. Abd El-Lateef, H.M., Khalaf, M.M., Mohamed, I.M., (2024), “XPS analysis, voltammetric, and impedance characteristics of novel heterogeneous biphosphates based on Cu/Ni for tri (ammonium) phosphate oxidation: a new direction for material processing in fuel technology”, *Fuel*, 356, 129618.
- [16]. Wang, D., Wang, Y., Fu, Z., Xu, Y., Yang, L. X., Wang, F., Yang, Z.L., (2021), “Cobalt–nickel phosphate composites for the all-phosphate asymmetric supercapacitor and oxygen evolution reaction”, *ACS applied materials & interfaces*, 13(29), 34507-34517.